

Cite this: *Nanoscale*, 2023, **15**, 12471

Received 19th June 2023,

Accepted 13th July 2023

DOI: 10.1039/d3nr02936k

rsc.li/nanoscale

## Detection of SO<sub>2</sub> using a chemically stable Ni(II)-MOF†

Valeria B. López-Cervantes,<sup>‡a</sup> Dae Won Kim,<sup>‡b</sup> Juan L. Obeso,<sup>‡a,c</sup>  
Eva Martínez-Ahumada,<sup>a</sup> Yoarhy A. Amador-Sánchez,<sup>a</sup> Elí Sánchez-González,<sup>‡a</sup>  
Carolina Leyva,<sup>‡c</sup> Chang Seop Hong,<sup>‡b</sup> Ilich A. Ibarra<sup>‡a</sup> and  
Diego Solís-Ibarra<sup>‡a</sup>

The MOF-type Ni<sub>2</sub>(dobpdc) shows a high chemical stability towards SO<sub>2</sub>, high capacity for SO<sub>2</sub> capture at low pressure (4.3 mmol g<sup>−1</sup> at 298 K and up to 0.05 bar), and exceptional cycling performance. Fluorescence experiments demonstrated the SO<sub>2</sub> detection properties of Ni<sub>2</sub>(dobpdc) with a remarkable SO<sub>2</sub> detection selectivity. Finally, time-resolved photoluminescence experiments provided a plausible mechanism of SO<sub>2</sub> detection by this Ni(II)-based MOF material.

## Introduction

Sulphur dioxide (SO<sub>2</sub>) is classified as one of the most toxic chemicals with a pungent odour. SO<sub>2</sub> is an irritant, colourless, irritating, and non-flammable gas easily absorbed by the respiratory system or dermal contact.<sup>1</sup> The presence of SO<sub>2</sub> is accountable for a direct rise in respiratory complications (e.g., broncho-constriction in lung function) and even death (contact over 100 ppm of SO<sub>2</sub> in only a few minutes).<sup>2</sup> Although it is naturally formed by volcanic activity, the main source of SO<sub>2</sub> is the combustion of fossil fuels containing sulphur and metal extraction from ores.<sup>3</sup> Moreover, SO<sub>2</sub> is a precursor of particulate matter (PM), another high threat to human health.<sup>4</sup> In addition, SO<sub>2</sub> is one of the principal constituents of acid rain, which negatively impacts aquatic environments and causes loss of minerals and nutrients from

the soil, hampering the growth of forests and crop plants.<sup>5</sup> Acid rain, in urban areas, drastically accelerates the corrosion of metallic structures and attacks the main constituents of buildings (e.g., limestone, marble, and mortar).<sup>6</sup> Thus, it becomes imperative to improve air quality, especially in urban areas, by reducing the emissions of SO<sub>2</sub> and identifying potentially polluted environments with SO<sub>2</sub>.

Most of the technological efforts toward SO<sub>2</sub> have been concentrated on capturing this toxic gas. For this, the most used technology for SO<sub>2</sub> capture is based on scrubbers.<sup>7</sup> However, this technology has demonstrated serious disadvantages such as low capture of SO<sub>2</sub>, vast quantities of wastewater, corrosion of pipelines, and considerable cost of use and recovery.<sup>8</sup> In addition, other solid-state materials (e.g., zeolites<sup>9</sup> and metal oxides<sup>10</sup>) have been investigated for the efficient capture of SO<sub>2</sub> with considerable drawbacks, such as high re-activation temperatures (above 250 °C) and a significant loss in porosity.<sup>11</sup> Unquestionably, the capture of SO<sub>2</sub> has shown to be a challenging task that requires new technological approaches.

A relatively new class of highly crystalline and porous materials known as metal-organic frameworks (MOFs) has been recently explored.<sup>12</sup> Selected examples have demonstrated remarkable SO<sub>2</sub> capture results,<sup>13</sup> even under humid conditions.<sup>14</sup> However, one of the main criticisms of MOFs is the current high cost of production for the organic ligands, in combination with difficult scalability, which raises questions about the sustainable economics of capturing SO<sub>2</sub> using MOFs at the industrial scale.

Interestingly, more research needs to be dedicated to detecting SO<sub>2</sub> with MOFs.<sup>15</sup> Conversely to SO<sub>2</sub> capture with MOFs, where large amounts of these materials are required, for the detection of SO<sub>2</sub>, only small amounts of a particular MOF material are needed.<sup>16</sup> Thus, detecting SO<sub>2</sub> is an extremely desirable characteristic for a MOF material to identify potentially polluted surroundings with this toxic gas. For example, if a chemically stable MOF material exhibits luminescence properties, the fluorescent response to SO<sub>2</sub> change would be the key to exploring such material as an effective SO<sub>2</sub> detector.

<sup>a</sup>Laboratorio de Fisicoquímica y Reactividad de Superficies (LaFREs), Instituto de Investigaciones en Materiales, Universidad Nacional Autónoma de México, Circuito Exterior s/n, CU, Coyoacán, 04510 Ciudad de México, Mexico.

E-mail: diego.solis@unam.mx, argel@unam.mx; Fax: +52 55 5622 4595

<sup>b</sup>Department of Chemistry, Korea University, Seoul 02841, Republic of Korea.

E-mail: cshong@korea.ac.kr

<sup>c</sup>Instituto Politécnico Nacional, CICATA U. Legaria, Laboratorio Nacional de Ciencia, Tecnología y Gestión Integrada del Agua (LNAgua), Legaria 694 Irrigación, Miguel Hidalgo, 11500 CDMX, Mexico

†Electronic supplementary information (ESI) available: Material characterisation, and photoluminescence experiments. See DOI: <https://doi.org/10.1039/d3nr02936k>

‡These authors contributed equally to this work.

Thus, with this specific target in mind, a robust and chemically stable Ni(II)-based MOF material entitled  $\text{Ni}_2(\text{dobpdc})$  was selected to address  $\text{SO}_2$  detection effectively.  $\text{Ni}_2(\text{dobpdc})$  MOF is constructed from the coordination of Ni(II) ions and 4,4'-dioxidobiphenyl-3,3'-dicarboxylate ( $\text{dobpdc}$ )<sup>4-</sup> ligand (Fig. S1†).<sup>17</sup> Each Ni(II) centre is hexa-coordinated to six O-donor atoms: in the equatorial plane, Ni(II) is coordinated to two *trans*-disposed bridgings ( $\mu_2$ ) aryloxy O atoms from two different  $\text{dobpdc}$  ligands to one bridging ( $\mu_2$ ) carboxylate O atom and one nonbridging carboxylate O atom. Also, from the ligand, whereas, in the axial plane, the Ni(II) centre is coordinated to one bridging ( $\mu_2$ ) carboxylate O atom from the ligand and a methanol (MeOH) molecule, which is used as a solvent in the solvothermal synthesis.<sup>18</sup> Such coordination array forms hexagonal helical chains across the *c*-axis of the crystal with a pore size of approximately 17 Å (Fig. S1†). After an activation process at 523 K for 12 h under vacuum ( $1.7 \times 10^{-3}$  Torr), coordinated MeOH molecules to Ni(II) metal centres are fully removed, providing uncoordinated  $\text{Ni}^{2+}$  sites.

Herein,  $\text{Ni}_2(\text{dobpdc})$  exhibited to be chemically stable to  $\text{SO}_2$ , with a total  $\text{SO}_2$  uptake of  $12.5 \text{ mmol g}^{-1}$ , at 298 K and 1 bar. Remarkably, solid-state fluorescence experiments demonstrated that  $\text{Ni}_2(\text{dobpdc})$  has proven to be an effective selective detector of this toxic pollutant.

Powder X-ray diffraction (PXRD) and thermogravimetric analysis (TGA) confirmed the phase purity of  $\text{Ni}_2(\text{dobpdc})$  (Fig. S2 and S3†). A sample of  $\text{Ni}_2(\text{dobpdc})$  was activated at 523 K for 12 h under vacuum ( $1.4 \times 10^{-3}$  torr). Then, an  $\text{N}_2$  isotherm at 77 K (Fig. S4†) demonstrated a BET surface area of  $3005 \text{ m}^2 \text{ g}^{-1}$  with a pore volume of  $1.11 \text{ cm}^3 \text{ g}^{-1}$ .

$\text{SO}_2$  adsorption-desorption isotherm using a Dynamic Gravimetric Gas/Vapour Sorption Analyser, DVS vacuum (Surface Measurement Systems Ltd), was carried out from 0 to 1 bar at 298 K on an activated sample of  $\text{Ni}_2(\text{dobpdc})$ . Fig. 1 shows the resulting isotherm obtained. A steep with fast  $\text{SO}_2$

uptake from 0.0 to 0.05 bar is noted, accounting for a total uptake of approximately  $4.3 \text{ mmol g}^{-1}$ . From 0.05 to 0.4 bar, the  $\text{SO}_2$  adsorption isotherm showed an approximate linear uptake with a total amount of  $\approx 9.4 \text{ mmol g}^{-1}$ . Finally, from 0.4 to 1.0 bar (end of the  $\text{SO}_2$  adsorption experiment), a slow  $\text{SO}_2$  uptake is observed. A total  $\text{SO}_2$  uptake of  $12.5 \text{ mmol g}^{-1}$  was achieved. This fully  $\text{SO}_2$  uptake is comparable to representative chemically stable MOFs.<sup>19</sup> Furthermore, the desorption isotherm shows a slight hysteresis, suggesting a relatively high  $\text{SO}_2$ /MOF interaction energy.

Possibly, the most significant property of a chemically stable MOF material toward  $\text{SO}_2$  detection is high  $\text{SO}_2$  adsorption at low pressure ( $P < 0.1$  bar). Considering that concentration ranges for  $\text{SO}_2$  detection are at the ppm level, these can be naturally correlated to the  $\text{SO}_2$  low-pressure range. Thus, the total  $\text{SO}_2$  uptake (at ambient pressure) becomes irrelevant. For example, flue gas displays  $\text{SO}_2$  concentrations up to 10 000 ppm, which is directly related to a pressure below 0.05 bar.<sup>20</sup>

Interestingly, at a very low pressure of only 0.002 bar,  $\text{Ni}_2(\text{dobpdc})$  captures  $1.98 \text{ mmol g}^{-1}$  of  $\text{SO}_2$  (Fig. 2). In this case, only four MOF materials surpassed this value:  $\text{Mg}_2(\text{dobpdc})$  ( $2.35 \text{ mmol g}^{-1}$ ),<sup>21</sup> Ni-gallate ( $4.25 \text{ mmol g}^{-1}$ ),<sup>22</sup> Mg-gallate ( $6.09 \text{ mmol g}^{-1}$ ),<sup>22</sup> and Co-gallate ( $6.13 \text{ mmol g}^{-1}$ ),<sup>22</sup> at 298 K. Thus, this  $\text{SO}_2$  capture at such low pressure is highly relevant for detecting  $\text{SO}_2$ .

Later, a structural stability test of  $\text{Ni}_2(\text{dobpdc})$  after the  $\text{SO}_2$  adsorption-desorption experiment was conducted. PXRD analysis confirmed the retention of the crystallinity (Fig. S5†) after the first  $\text{SO}_2$  sorption experiment. Moreover, an  $\text{N}_2$  adsorption isotherm at 77 K demonstrated that the porosity is not modified (BET area  $\approx 3005 \text{ m}^2 \text{ g}^{-1}$ , Fig. S6†).

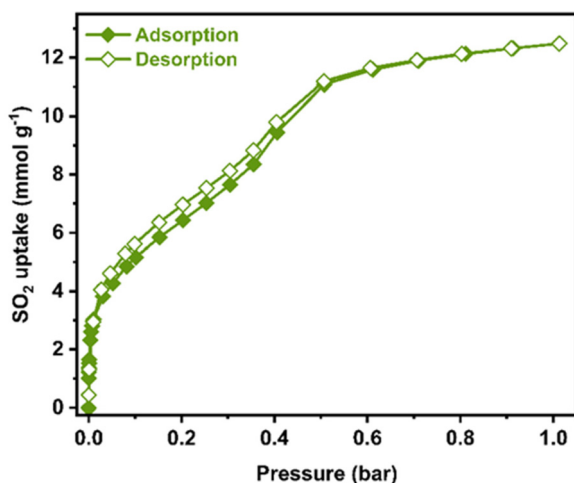


Fig. 1 Experimental  $\text{SO}_2$  adsorption-desorption isotherm collected for a fully activated  $\text{Ni}_2(\text{dobpdc})$  sample (filled green diamonds = adsorption; open green diamonds = desorption) at 298 K and up to 1 bar.

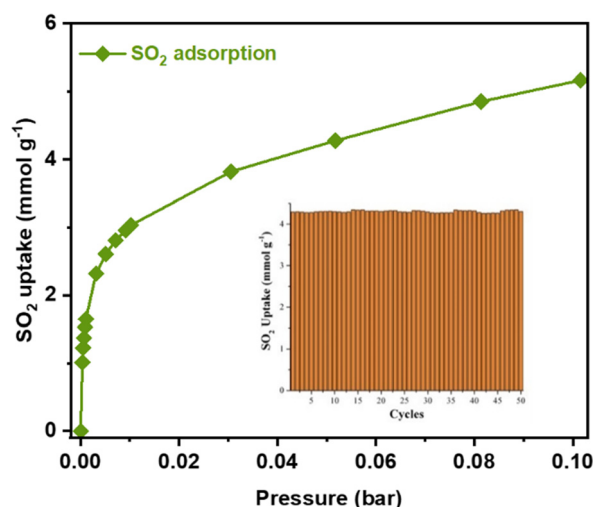


Fig. 2 Experimental  $\text{SO}_2$  adsorption isotherm collected for a fully activated  $\text{Ni}_2(\text{dobpdc})$  sample at 298 K and up to 0.1 bar. Inset: Adsorption-desorption cycles for  $\text{SO}_2$  in  $\text{Ni}_2(\text{dobpdc})$  at 0.05 bar and 298 K. The re-activation of the sample was performed by only operating under a vacuum ( $1.7 \times 10^{-3}$  torr) for 45 minutes at room temperature (298 K).

Moreover, the host–guest interaction ( $\text{SO}_2\text{--Ni}_2(\text{dobpdc})$ ) was quantified by calculating the isosteric heat of adsorption ( $\Delta H$ ) for  $\text{SO}_2$  at low coverage for a fully activated sample of  $\text{Ni}_2(\text{dobpdc})$  (two adsorption isotherms at 298 and 308 K were fitted to a Clausius–Clapeyron equation, Fig. S7†). Then, the calculated  $\Delta H = -95.2 \text{ kJ mol}^{-1}$  was demonstrated to be relatively high, suggesting a relatively strong interaction between  $\text{SO}_2$  and the walls of the MOF material. This  $\Delta H$  value is also consistent with the hysteresis shown in Fig. 1. It is characteristic of  $\text{SO}_2$  and open metal site systems (e.g.,  $\text{Mg}_2(\text{dobpdc})$ ,<sup>21</sup>  $\Delta H = -90.0 \text{ kJ mol}^{-1}$ ). Also, it is observed a decrease in  $\Delta H$  (Fig. S7†) when the  $\text{SO}_2$  loading is increased. Thus, open metal sites are first occupied by  $\text{SO}_2$  (higher energy binding sites), and then, at higher loadings, the  $\text{SO}_2$  molecule interacts through intermolecular forces with the pore walls of the MOF.

Therefore, cycling  $\text{SO}_2$  experiments at 298 K and 0.05 bar were further investigated in order to evaluate the stability of the  $\text{SO}_2$  adsorption–desorption performance and the regeneration capacity of  $\text{Ni}_2(\text{dobpdc})$  by simply applying vacuum ( $1.7 \times 10^{-3}$  Torr) for 45 minutes and 298 K. Thus, it was shown that the  $\text{SO}_2$  capture capacity, at very low pressure, constantly continued for 50 adsorption–desorption cycles ( $4.31 \pm 0.10 \text{ mmol g}^{-1}$ , Fig. 2, inset). This shows that  $\text{SO}_2$  is fully released during the subsequent desorption cycles. Also, PXRD analyses of the material after 50 adsorption/desorption cycles confirmed the retention of the crystal structure (Fig. S5†). At the same time,  $\text{N}_2$  adsorption isotherm at 77 K evidenced that the porosity was not modified (BET area  $\approx 3005 \text{ m}^2 \text{ g}^{-1}$ , Fig. S6†). This result exhibits that  $\text{SO}_2$  can be fully released when  $\text{SO}_2$  cycle experiments are carried out without modifying the crystal structure of  $\text{Ni}_2(\text{dobpdc})$ .

Up to this point, the  $\text{SO}_2$  capture by  $\text{Ni}_2(\text{dobpdc})$ , particularly at very low pressure (0.002 bar), has been demonstrated. This is a fundamental requirement for  $\text{SO}_2$  detection.  $\text{Ni}_2(\text{dobpdc})$  also showed high  $\text{SO}_2$  cyclability and extraordinary chemical stability to  $\text{SO}_2$ , desirable characteristics for  $\text{SO}_2$  detection.

Thus, another fundamental aspect of any detector is selectivity.<sup>23</sup> A  $\text{CO}_2$  single-component adsorption isotherm was collected at 298 K and 1 bar (Fig. S9†). The  $\text{SO}_2$  adsorbed amount in  $\text{Ni}_2(\text{dobpdc})$  was higher than the  $\text{CO}_2$  in the whole pressure range. Then, we calculated the selectivity of  $\text{SO}_2$  over  $\text{CO}_2$  at different compositions ( $\text{SO}_2/\text{CO}_2$ ) using the Python package (Table S1†), pyIAST,<sup>24</sup> corroborating a remarkable  $\text{SO}_2/\text{CO}_2$  selectivity by  $\text{Ni}_2(\text{dobpdc})$ .

Once it was comprehensively established that the  $\text{SO}_2$  adsorption characteristics of  $\text{Ni}_2(\text{dobpdc})$  as a promising  $\text{SO}_2$  detector, the possibility of using this MOF material as a fluorescent  $\text{SO}_2$  detector was investigated, first, under UV light irradiation at  $\lambda_{\text{ex}} = 350 \text{ nm}$  (Fig. S12†), an activated sample of  $\text{Ni}_2(\text{dobpdc})$  showed a broad photoluminescence peak centred at  $\lambda_{\text{max}} = 450 \text{ nm}$ , as it is observed in Fig. 3. This is attributed to the *dobpdc* fragment as previously reported for  $\text{Mg}_2(\text{dobpdc})$ .<sup>21</sup> Then, another activated sample of  $\text{Ni}_2(\text{dobpdc})$  was exposed (saturated) to  $\text{SO}_2$  in our homemade *in situ* adsorption system (Fig. S8†) to measure its photoluminescence



Fig. 3 Solid-state emission spectra of activated  $\text{Ni}_2(\text{dobpdc})$  (green) and after exposure to  $\text{SO}_2$  (yellow),  $\text{CO}_2$  (red), and  $\text{H}_2\text{O}$  (blue).

absorption properties of it later. Interestingly, the photoluminescence shifts to 405 nm and an increase of approximately 61 % in emission intensity was observed.

These photoluminescence changes in position and intensity can be attributed to the electronic effect that  $\text{SO}_2$  applies on the framework when coordinated to the Ni-centres, which is successively transferred to the *dobpdc* ligand. A control experiment was conducted further to test the selectivity of  $\text{Ni}_2(\text{dobpdc})$ . The fluorescence of  $\text{Ni}_2(\text{dobpdc})$  upon exposure to  $\text{H}_2\text{O}$  and  $\text{CO}_2$  was measured (Fig. 3). Importantly, none of these molecules generated significant changes in the shape or intensity of the photoluminescence compared to the spectrum of activated  $\text{Ni}_2(\text{dobpdc})$ .

Thus, since none of these conditions (exposure to  $\text{H}_2\text{O}$  and  $\text{CO}_2$ ) significantly altered the shape or intensity of the emission, corroborated the selectivity of  $\text{Ni}_2(\text{dobpdc})$  to  $\text{SO}_2$ , indicating that the change in fluorescence is exclusively due to  $\text{SO}_2$  adsorption-coordination and not due to other molecules. Later, five independent experiments were measured. An activated  $\text{Ni}_2(\text{dobpdc})$  sample was saturated with  $\text{SO}_2$ . Consistently, it was found that the same absorption spectrum shifted to 405 nm, with an approximate 61 % increase in emission intensity.

Once it was demonstrated the  $\text{SO}_2$  detection selectivity for  $\text{Ni}_2(\text{dobpdc})$ , over  $\text{H}_2\text{O}$  and  $\text{CO}_2$ , and the reproducibility of the detection of saturated samples  $\text{Ni}_2(\text{dobpdc})$  with  $\text{SO}_2$ , the detection properties of this Ni(II)-based material at low  $\text{SO}_2$  pressure: non-saturated  $\text{Ni}_2(\text{dobpdc})$  with  $\text{SO}_2$  was investigated. Since  $\text{Ni}_2(\text{dobpdc})$  demonstrated a relatively high  $\text{SO}_2$  uptake at low pressure ( $P = 0.1 \text{ bar}$ , *vide supra*), and this low pressure can be correlated to  $\text{SO}_2$  detection at low  $\text{SO}_2$  concentrations, it becomes crucial to investigate photoluminescence response at lower  $\text{SO}_2$  pressures (in this case, 0.1 bar).

Thus, an activated sample of  $\text{Ni}_2(\text{dobpdc})$  was exposed to 0.1 bar of  $\text{SO}_2$  (Fig. S8†). The emission spectrum was measured

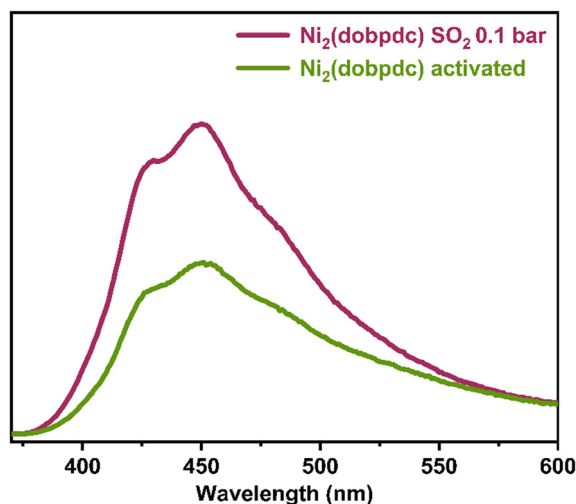


Fig. 4 Comparison of solid-state emission spectra of  $\text{Ni}_2(\text{dobpdc})$  samples activated (green) and exposed to  $\text{SO}_2$  at 0.1 bar (pink).

(Fig. 4). Interestingly, the broad photoluminescence peak remained centred at  $\lambda_{\text{max}} = 450$  nm. An increase in emission intensity of approximately 62 % was observed. Also, the reproducibility of this experiment was evaluated with 5 independent experiments (re-activation of the sample and re-exposure to 0.1 bar of  $\text{SO}_2$ ). It was found that an increase of approximately 62 % in emission intensity. It is worth mentioning that only the  $\text{SO}_2$  detection by  $\text{Ni}_2(\text{dobpdc})$  at 0.1 bar was performed. At this point, it cannot be translated to  $\text{SO}_2$  sensing. Although we consistently found an increase in the emission intensity when re-exposing to  $\text{SO}_2$  and re-activating the sample of  $\text{Ni}_2(\text{dobpdc})$  at 0.1 bar  $\text{SO}_2$ . Nevertheless, it is not possible to quantify the precise amount of  $\text{SO}_2$  by photoluminescence. However, achieving a consistent and reproducible response is very promising when this  $\text{Ni}(\text{II})$ -based MOF material is exposed to 0.1 or 1 bar of  $\text{SO}_2$ .

Finally, in order to investigate the plausible mechanism of  $\text{SO}_2$  detection by  $\text{Ni}_2(\text{dobpdc})$ , a time-resolved photoluminescence (TRPL) experiment was performed using a 340 nm picosecond-pulsed LED as the excitation source (Fig. 5). TRPL experiments were carried out on an activated sample of  $\text{Ni}_2(\text{dobpdc})$  and an  $\text{SO}_2$ -saturated sample. The photoluminescence decay was measured at three different emission wavelengths: 405 nm, which was the emission maximum of the  $\text{SO}_2$ -saturated sample; 450 nm, corresponding to the emission maximum of the activated sample and 425 nm since this signal was observed in both spectra (Fig. S13–S16†). For all three emission wavelengths, it was observed that the average decay lifetimes increased upon  $\text{SO}_2$  exposure (Table S2†). Thus, the average fluorescence lifetime of the activated sample (at  $\lambda_{\text{emission}} = 405$  nm) was 2.14 ns, while the lifetime of the  $\text{SO}_2$ -saturated sample (at  $\lambda_{\text{emission}} = 405$  nm) was 2.47 ns (Fig. 5). These results suggest that the coordination of  $\text{SO}_2$  molecules to the  $\text{Ni}(\text{II})$  metal centres rigidify the molecular motions of the organic ligand (dobpdc). Subsequently, it hinders non-radiative decay pathways of the photoexcited state, causing the fluorescence lifetime to slow



Fig. 5 Time-resolved photoluminescence decay spectra of activated  $\text{Ni}_2(\text{dobpdc})$ , and after exposure to  $\text{SO}_2$  measured at 405 nm at 340 nm excitation.

down. Thus, it increases the number of radiatively decaying excited species, leading to an improvement in the fluorescence intensity.<sup>25</sup>

One of the reasons why the wavelength shifts, is the change in energy due to the electronic transitions, where intermolecular interactions can considerably influence. It was previously reported that a strong interaction could considerably impact the excited state of some materials.<sup>26</sup> Thus, this can indicate that the coordination of  $\text{SO}_2$  to all the  $\text{Ni}(\text{II})$  centres is strong enough to increase the energy difference between the basal and excited states, causing the fully  $\text{SO}_2$ -coordinated  $\text{Ni}_2(\text{dobpdc})$  to emit light at higher energies. In other words, a shift in the spectrum can be observed at higher energies, *i.e.*, at shorter wavelengths.

To summarise, the  $\text{SO}_2$  adsorption and detection properties of a structurally stable MOF material entitled  $\text{Ni}_2(\text{dobpdc})$  were investigated.  $\text{Ni}_2(\text{dobpdc})$  demonstrated a high  $\text{SO}_2$  uptake at low pressure ( $4.3 \text{ mmol g}^{-1}$  at 298 K and 0.05 bar), in combination with an excellent cyclability performance with a facile  $\text{SO}_2$  regeneration at room temperature. Fluorescence studies exhibited a significant change in the emission spectra after  $\text{SO}_2$  adsorption, with a clear  $\text{SO}_2$  detection selectivity, over  $\text{H}_2\text{O}$  and  $\text{CO}_2$  and reproducible  $\text{SO}_2$  response when this  $\text{Ni}(\text{II})$ -based MOF material was exposed to only 0.1 or 1 bar of  $\text{SO}_2$ . Finally, time-resolved photoluminescence experiments suggested that the coordination of  $\text{SO}_2$  molecules to the  $\text{Ni}(\text{II})$  metal centres rigidify the molecular motions of the organic ligand (dobpdc), leading to an increase in fluorescence intensity. Overall, this study postulates  $\text{Ni}_2(\text{dobpdc})$  as a promising candidate for  $\text{SO}_2$  detection.

## Conflicts of interest

There are no conflicts to declare.



## Acknowledgements

V. B. L.-C. and J. L. O. thank CONACYT for the Ph.D. fellowship (1005649, 1003953). The authors thank Dr. A. Tejeda-Cruz (powder X-ray; IIM-UNAM), PAPIIT UNAM (IN201123), México, for financial support. Thanks to U. Winnberg (Euro Health) for scientific discussions and G. Ibarra-Winnberg for conceptualising the design of this contribution. C. S. Hong also acknowledged financial support from the National Research Foundation of Korea (NRF-2021R1A2B5B03086313 and NRF-2019R1A6A1A11044070).

## References

- 1 Z. Klimont, S. J. Smith and J. Cofala, *Environ. Res. Lett.*, 2013, **8**, 014003.
- 2 M. Matooane and R. Diab, *Arch. Environ. Health*, 2003, **58**, 763–770.
- 3 P. Amoatey, H. Omidvarborna, M. S. Baawain and A. Al-Mamun, *Process Saf. Environ. Prot.*, 2019, **123**, 215–228.
- 4 J. Schwartz and D. W. Dockery, *Am. Rev. Respir. Dis.*, 1992, **145**, 600–604.
- 5 R. Reiss, E. L. Anderson, C. E. Cross, G. Hidy, D. Hoel, R. McClellan and S. Moolgavkar, *Inhalation Toxicol.*, 2007, **19**, 419–449.
- 6 F. C. Menz and H. M. Seip, *Environ. Sci. Policy*, 2004, **7**, 253–265.
- 7 R. K. Srivastava, W. Jozewicz and C. Singer, *Environ. Prog.*, 2001, **20**, 219–228.
- 8 B. E. Alver, M. Sakizci and E. Yörükoğullari, *Adsorpt. Sci. Technol.*, 2011, **29**, 413–422.
- 9 B. Erdoğan Alver, *J. Hazard. Mater.*, 2013, **262**, 627–633.
- 10 N. D. Hutson, B. A. Reisner, R. T. Yang and B. H. Toby, *Chem. Mater.*, 2000, **12**, 3020–3031.
- 11 A. J. Hernández-Maldonado, R. T. Yang, D. Chinn and C. L. Munson, *Langmuir*, 2003, **19**, 2193–2200.
- 12 W. Lu, Z. Wei, Z.-Y. Gu, T.-F. Liu, J. Park, J. Park, J. Tian, M. Zhang, Q. Zhang, T. Gentle III, M. Bosch and H.-C. Zhou, *Chem. Soc. Rev.*, 2014, **43**, 5561–5593.
- 13 A. López-Olvera, S. Pioquinto-García, J. Antonio Zárate, G. Diaz, E. Martínez-Ahumada, J. L. Obeso, V. Martis, D. R. Williams, H. A. Lara-García, C. Leyva, C. V. Soares, G. Maurin, I. A. Ibarra and N. E. Dávila-Guzmán, *Fuel*, 2022, **322**, 124213.
- 14 A. López-Olvera, J. A. Zárate, E. Martínez-Ahumada, D. Fan, M. L. Díaz-Ramírez, P. A. Sáenz-Cavazos, V. Martis, D. R. Williams, E. Sánchez-González, G. Maurin and I. A. Ibarra, *ACS Appl. Mater. Interfaces*, 2021, **13**, 39363–39370.
- 15 J. L. Obeso, E. Martínez-Ahumada, A. López-Olvera, J. Ortiz-Landeros, H. A. Lara-García, J. Balmaseda, S. López-Morales, E. Sánchez-González, D. Solis-Ibarra, C. Leyva and I. A. Ibarra, *ACS Appl. Energy Mater.*, 2020, DOI: [10.1021/acsaem.2c02983](https://doi.org/10.1021/acsaem.2c02983).
- 16 S. Yang, J. Sun, A. J. Ramirez-Cuesta, S. K. Callear, W. I. F. David, D. P. Anderson, R. Newby, A. J. Blake, J. E. Parker, C. C. Tang and M. Schröder, *Nat. Chem.*, 2012, **4**, 887–894.
- 17 T. M. McDonald, J. A. Mason, X. Kong, E. D. Bloch, D. Gygi, A. Dani, V. Crocellà, F. Giordanino, S. O. Odoh, W. S. Drisdell, B. Vlasisavljevich, A. L. Dzubak, R. Poloni, S. K. Schnell, N. Planas, K. Lee, T. Pascal, L. F. Wan, D. Prendergast, J. B. Neaton, B. Smit, J. B. Kortright, L. Gagliardi, S. Bordiga, J. A. Reimer and J. R. Long, *Nature*, 2015, **519**, 303–308.
- 18 (a) D. Gygi, E. D. Bloch, J. A. Mason, M. R. Hudson, M. I. Gonzalez, R. L. Siegelman, T. A. Darwish, W. L. Queen, C. M. Brown and J. R. Long, *Chem. Mater.*, 2016, **28**, 1128–1138; (b) T. M. McDonald, W. R. Lee, J. A. Mason, B. M. Wiers, C. S. Hong and J. R. Long, *J. Am. Chem. Soc.*, 2012, **134**(16), 7056–7065.
- 19 J. H. Carter, X. Han, F. Y. Moreau, I. da Silva, A. Nevin, H. G. W. Godfrey, C. C. Tang, S. Yang and M. Schröder, *J. Am. Chem. Soc.*, 2018, **140**(46), 15564–15567.
- 20 P. Brandt, S.-H. Xing, J. Liang, G. Kurt, A. Nuhnen, O. Weingart and C. Janiak, *ACS Appl. Mater. Interfaces*, 2021, **13**, 29137–29149.
- 21 E. Martínez-Ahumada, D. won Kim, M. Wahiduzzaman, P. Carmona-Monroy, A. López-Olvera, D. R. Williams, V. Martis, H. A. Lara-García, S. López-Morales, D. Solis-Ibarra, G. Maurin, I. A. Ibarra and C. S. Hong, *J. Mater. Chem. A*, 2022, **10**, 18636–18643.
- 22 F. Chen, D. Lai, L. Guo, J. Wang, P. Zhang, K. Wu, Z. Zhang, Q. Yang, Y. Yang, B. Chen, Q. Ren and Z. Bao, *J. Am. Chem. Soc.*, 2021, **143**, 9040–9047.
- 23 K. Tan, S. Zuluaga, H. Wang, P. Canepa, K. Soliman, J. Cure, J. Li, T. Thonhauser and Y. J. Chabal, *Chem. Mater.*, 2017, **29**, 4227–4235.
- 24 C. M. Simon, B. Smit and M. Haranczyk, *Comput. Phys. Commun.*, 2016, **200**, 364–380.
- 25 L. E. Kreno, K. Leong, O. K. Farha, M. Allendorf, R. P. Van Duyne and J. T. Hupp, *Chem. Rev.*, 2012, **112**, 1105–1125.
- 26 A. P. Demchenko, *Introduction to Fluorescence Sensing*, Springer, Switzerland, 2015, ch. 3, pp. 69–126.